Advanced Computational Methods in Heat Transfer II

Vol. 2: Natural/Forced Convection and Combustion Simulation

Editors: L.C. Wrobel, Wessex Institute of Technology, University of Portsmouth, UK
C.A. Brebbia, Wessex Institute of Technology, University of Portsmouth, UK
A.J. Nowak, Silesian Technical University, Poland

Computational Mechanics Publications
Southampton Boston

Co-published with

Elsevier Applied Science
London New York

Film-Cooling of Gas Turbine Combustion Chamber Walls: A Numerical Study Using a Two-Layer Algebraic Stress Model

S. Jansson, L. Davidson, E. Olsson
Department of Thermo and Fluid Dynamics,
Chalmers University of Technology,
S-412 96 Gothenburg, Sweden

ABSTRACT

In recent years there has been a growing interest in ceramic materials for high-temperature gas turbine chambers. Owing to different material properties, these gas turbine chambers have thicker walls than the metallic ones, which gives a different geometry of the film-cooling slots, and hence the flow field will be affected. In this work the mean and fluctuating velocities and fluid temperatures have been studied numerically for two different lip-to-slot-ratios. When the lip is thick, the flow becomes unsteady and a vortex street appears behind the lip, and hence unsteady computations have been carried out. The calculated results are compared with recently made hot-wire measurements by Boman [1].

INTRODUCTION

The purpose of this investigation is to model both the flow and temperature fields numerically, and to examine the validity of the eddy-viscosity concept and of an algebraic-stress-model at different slot-lip-thickness and flow ratios in a two-dimensional slot with tangential injection, and to relate the results to the wake flow characteristics downstream of the lip. Launder & Rodi [10] examined how well current calculation schemes succeed in mimicking the measured behavior of turbulent wall jets. They found out that the models derived from the Reynolds transport stress transport equation (whether of a full **R**eynolds **S**tress **M**odel **RSM** or an **A**lgebraic **S**tress **M**odel **ASM** form) were more successful than the Boussinesq stress-strain relation in imitating the wall jet's behavior, and that a crucial element in these closures is the modelling of turbulent pressure reflections from the wall: it is this process that is responsible for the slower growth rate of the plane wall jet than the free jet.

In most works in the literature, except Kacker [7] who used an elliptic steady solver, parabolic solvers have been used. However, in the present

study when the lip was thick (t/s = 1.0), a periodic von Kárman vortex street was obtained behind the lip, because of which the flow field became unsteady and elliptic. In a review by Rodi [17], calculations with both a full **RSM**, an **ASM** and the $k - \varepsilon$ model were presented for a vortex-shedding flow past a circular cylinder. Their results were in better agreement with the data when the Reynolds stress equation models (**RSM** or **ASM**) were used. A conclusion was that the assumption of the eddy-viscosity as a scalar quantity in the $k - \varepsilon$ model is invalid, and that a Reynolds stress equation model is necessary for a realistic simulation of this motion. Also, a conclusion was that a good numerical resolution in the near-wall region is essential for a realistic simulation of vortex shedding.

The present calculations have been made, comparing two different discretization schemes for the convective terms, using both an **ASM**, in order to better predict the anisotropy effects of the turbulence, and the standard $k - \varepsilon$ model. These two high Reynolds number models have been combined with a one-equation model by Norris and Reynolds [13] near the walls in order to account for the viscous effects on the turbulence. The configurations considered, are relevant to high-temperature gas turbine chambers, see **Figure 1** below.

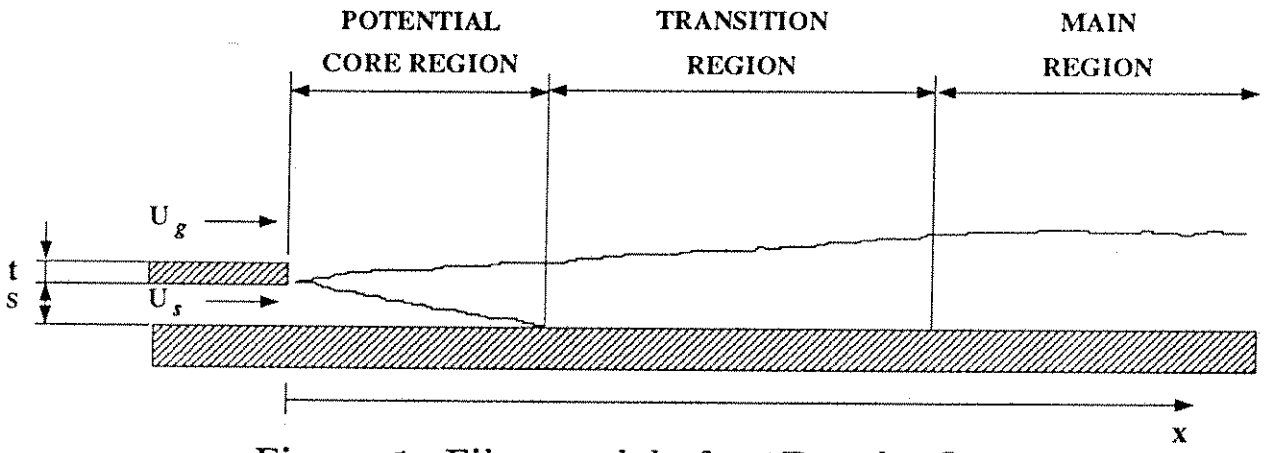

Figure 1. Film model of a 2D wake flow.

THE MEAN FLOW EQUATIONS

In Cartesian tensor notation, the time-averaged conservation equations for an incompressible unsteady flow without body forces can be expressed as:

Conservation of mass (Continuity equation)

$$\frac{\partial U_i}{\partial x_i} = 0 \qquad (1)$$

Conservation of momentum (Transport equation)

$$\frac{\partial}{\partial t}(\rho U_i) + \frac{\partial}{\partial x_j}(\rho U_j U_i) = -\frac{\partial P}{\partial x_i} + \frac{\partial \tau_{ij}}{\partial x_j} \tag{2}$$

where the stress tensor, τ_{ij} is written as:

$$\tau_{ij} = \mu\left(\frac{\partial U_i}{\partial x_j} + \frac{\partial U_j}{\partial x_i}\right) - \rho\overline{u_i u_j} \tag{3}$$

The $k-\varepsilon$ Model

The commonest way to model the Reynolds stresses is based on the eddy-viscosity concept according to Boussinesq:

$$-\rho\overline{u_i u_j} = \mu_t\left(\frac{\partial U_i}{\partial x_j} + \frac{\partial U_j}{\partial x_i}\right) - \frac{2}{3}\delta_{ij}\rho k \tag{4}$$

This concept assumes that the Reynolds stresses are proportional to the local mean velocity gradients and that the proportionality factor, the eddy viscosity, μ_t , is a scalar quantity, i.e. that is the same for all components of $\overline{u_i u_j}$. The eddy (turbulent) viscosity is calculated as:

$$\mu_t = C_\mu \rho \frac{k^2}{\varepsilon} \tag{5}$$

where C_μ is a constant. The spatial and temporal distribution of turbulent kinetic energy k and the dissipation rate ε are governed by two differential transport equations as follows:

$$\rho\frac{\partial k}{\partial t} + \frac{\partial}{\partial x_i}(\rho U_i k) = \frac{\partial}{\partial x_i}\left[\left(\mu + \frac{\mu_t}{\sigma_k}\right)\frac{\partial k}{\partial x_i}\right] + P_k - \rho\varepsilon \tag{6}$$

$$\rho\frac{\partial \varepsilon}{\partial t} + \frac{\partial}{\partial x_i}(\rho U_i \varepsilon) = \frac{\partial}{\partial x_i}\left[\left(\mu + \frac{\mu_t}{\sigma_\varepsilon}\right)\frac{\partial \varepsilon}{\partial x_i}\right] + \frac{\varepsilon}{k}\left[\, c_{\varepsilon 1} P_k - c_{\varepsilon 2}\rho\varepsilon \,\right] \tag{7}$$

where the production term, P_k and the constants can be written as:

$$P_k = \mu_t\left(\frac{\partial U_i}{\partial x_j} + \frac{\partial U_j}{\partial x_i}\right)\frac{\partial U_i}{\partial x_j} \tag{8}$$

$$\sigma_k = 1.0, \quad \sigma_\varepsilon = 1.3, \quad c_\mu = 0.09, \quad c_{\varepsilon 1} = 1.44, \quad c_{\varepsilon 2} = 1.92$$

The Algebraic Stress Model (ASM)

The algebraic stress model can be arrived at by making an assumption that the transport of the Reynolds stresses $\overline{u_i u_j}$ is proportional to the transport of turbulent kinetic energy k, i.e.

$$C_{ij} - D_{ij} = \frac{\overline{u_i u_j}}{k}(C_k - D_k) \tag{9}$$

where C_{ij}, D_{ij} represent the convective and diffusive transport of $\overline{u_i u_j}$ and C_k, D_k represent the corresponding terms for k. The ASM representation of the Reynolds stresses can after some algebraic manipulation be expressed in the following explicit form:

$$\overline{u_i u_j} = \frac{2}{3}\delta_{ij}k + \frac{k}{\varepsilon}\frac{(1-c_2)(P_{ij} - \frac{2}{3}\delta_{ij}P_k) + \phi_{ij,w}}{c_1 + P_k/\varepsilon - 1} \tag{10}$$

where P_{ij} and P_k denote the production of $\overline{u_i u_j}$ and k. These terms are exact and do not have to be modelled and are given as:

$$P_{ij} = -\rho\overline{u_i u_k}\frac{\partial U_j}{dx_k} - \rho\overline{u_j u_k}\frac{\partial U_i}{dx_k} \;\; ; \;\; P_k = -\rho\overline{u_i u_j}\frac{\partial U_i}{dx_j} \tag{11}$$

The pressure-strain correlation Φ_{ij}, involves correlations between fluctuating pressure and strain rates, and has to be modelled. Three processes contribute to the pressure-strain correlation, one "slow" term attributable only to the interaction of fluctuating velocities ($\phi_{ij,1}$), one "rapid" term arising from the interaction of mean strain and fluctuating velocities ($\phi_{ij,2}$), and one attributable to the effects of rigid boundaries ($\phi_{ij,w}$). Each contribution can be modelled separately [18] as follows:

$$\Phi_{ij} = \phi_{ij,1} + \phi_{ij,2} + \phi_{ij,w} \tag{12}$$

The 'slow' stress-isotropization term $\phi_{ij,1}$, proposed by Rotta [19], and the 'rapid' isotropization-of-production term $\phi_{ij,2}$, suggested by Naot *et al.* [12], are determined from:

$$\phi_{ij,1} = -c_1\frac{\varepsilon}{k}\left[\overline{u_i u_j} - \frac{2}{3}\delta_{ij}\,k\right] \;\; ; \;\; \phi_{ij,2} = -c_2\left[P_{ij} - \frac{2}{3}\delta_{ij}\,P_k\right] \tag{13}$$

The third term $\phi_{ij,w}$ represents the redistribution due to the effects of rigid boundaries on both $\phi_{ij,1}$ and $\phi_{ij,2}$ and is given by the sum of $\phi'_{ij,1}$ and $\phi'_{ij,2}$ which are, respectively, the near-wall corrections to $\phi_{ij,1}$ and $\phi_{ij,2}$, thus:

$$\phi_{ij,w} = \phi'_{ij,1} + \phi'_{ij,2} \tag{14}$$

where:

$$\phi'_{ij,1} = c'_1 \frac{\varepsilon}{k}\left[\overline{u_k u_m} n_k n_m \delta_{ij} - \frac{3}{2}\overline{u_k u_i} n_k n_j - \frac{3}{2}\overline{u_k u_j} n_k n_i\right] \cdot f_\ell \quad (15)$$

$$\phi'_{ij,2} = c'_2\left[\phi_{km,2} n_k n_m \delta_{ij} - \frac{3}{2}\phi_{ik,2} n_k n_j - \frac{3}{2}\phi_{jk,2} n_k n_i\right] \cdot f_\ell \quad (16)$$

where n_i is the unit vector in the "i"-direction normal to the wall (if present). The function f_ℓ is a damping function, more detailed described in [5], which reduces the effect of the wall correction with increasing distance from the wall.

At high Reynolds number, most of the viscous dissipation occurs at the small scales, which means that the dissipation term ε_{ij} can be assumed to be isotropic so that the same amount of energy is dissipated in each energy component $\overline{u_i^2}$ and hence it can be written as:

$$\varepsilon_{ij} = \frac{2}{3}\varepsilon\delta_{ij} \quad (17)$$

Finally, the model is closed by solving the transport equations for the turbulent kinetic energy, Equation (6) and its dissipation rate, Equation (7) with the production term P_k replaced with the exact expression in Equation (11), and the diffusive terms replaced with the more general relations:

$$(DIFF)_k = \frac{\partial}{\partial x_j}\left(\mu \frac{\partial k}{\partial x_j} + c_s \rho \overline{u_i u_j} \frac{k}{\varepsilon}\frac{\partial k}{\partial x_i}\right) \quad (18)$$

$$(DIFF)_\varepsilon = \frac{\partial}{\partial x_j}\left(\mu \frac{\partial \varepsilon}{\partial x_j} + c_{\varepsilon 3} \rho \overline{u_i u_j} \frac{k}{\varepsilon}\frac{\partial \varepsilon}{\partial x_i}\right) \quad (19)$$

NEAR-WALL TREATMENT

The Two-Layer Model

A two-layer model combines the actual high Reynolds number turbulence model with a simpler, but more reliable one-equation model to accurately resolve the flow near a solid wall. It separates the flow field into an outer region, where the viscous effects are small, and into an inner region where the viscous effects cannot be neglected. In the outer region, where the turbulent Reynolds number is high, the transport equations for all the dependent variables are solved as usual. The viscous-affected inner region, which includes the sublayer, the buffer layer and part of the fully turbulent layer, is

resolved with the one equation model. In this inner region, the dissipation rate ε, is not determined from a transport equation but from a prescribed length-scale distribution. Since the **ASM** is not valid in this inner region, the Reynolds stresses are here computed using the Boussinesq assumption, i.e. Equation (4). The one-equation model which has been chosen in this investigation is the one proposed by Norris and Reynolds [13]. The expression for the eddy viscosity in the inner region, ν_t is given as:

$$\nu_t = c_\mu \, k^{1/2} \, \ell_\mu \tag{20}$$

and ε is determined from:

$$\varepsilon = \frac{k^{3/2}}{\ell_\varepsilon} \tag{21}$$

Close to a wall the turbulent energy k decreases, owing to the damping of the turbulent stresses, and hence the eddy viscosity ν_t goes to zero. The damping of the eddy viscosity in this inner region is affected by a reduction of ℓ_μ, due to an exponential function similar to the van Driest damping function used in the mixing length theory. The Norris-Reynolds model employs the following expression for ℓ_μ:

$$\ell_\mu = C_\ell \, n \left[1 - exp\left(-\frac{Re_n}{A_\mu} \right) \right] \tag{22}$$

where n is the normal distance from the wall. The turbulent Reynolds number Re_n is given as:

$$Re_n = \frac{k^{1/2} n}{\nu} \tag{23}$$

which, in contrast to the original van Driest function, does not involve the friction velocity u^* and hence is valid also in cases with separated flows. The constant C_ℓ is chosen as:

$$C_\ell = \kappa \, C_\mu^{-3/4} \tag{24}$$

where C_μ is the same constant as in the standard $k - \varepsilon$ model (= 0.09) and κ is the von Kárman constant which is somewhat different for different modellers. The damping constant A_μ was determined from numerical tests and set to A_μ=50.5 [15]. The length-scale ℓ_ε in the expression for the dissipation rate (Equation (21)) is given as:

$$\ell_\varepsilon = \frac{C_\ell \, n}{1 + 5{\cdot}3/Re_n} \tag{25}$$

The one-equation model in the inner region must be matched with the high Reynolds number model in the outer region at some location in the flow. This location should be placed in a region where the viscous effects have become negligible. There are different ways of doing this. In this study, the matching took place where the damping function in the length-scale relation (Equation (22)), i.e. the expression in brackets, has a value close to unity, which means that the viscous effects are small. For the present calculations a value of 0.95 was chosen.

BOUNDARY CONDITIONS

Inlet

The inlet was located two slot-heights upstream of the rear edge of the lip and mean velocities, velocity fluctuations and the temperature were set according to the experiments. The dissipation rate was calculated from the expression in Equation (21) and the turbulent kinetic energy was calculated as:

$$k = \frac{1}{2}[\,\overline{u^2} + \overline{v^2} + \overline{w^2}\,] \tag{26}$$

Outlet

The exit velocity was set according to global mass balance between in- and outlet, and a zero streamwise gradient was imposed for the remaining variables.

Symmetry

A zero gradient was imposed for all variables except for the V-velocity, which was set to zero.

Blockage

A blocked region is situated inside the lip and all quantities there were set to zero, except for P, T and ϵ which were extrapolated from the interior flow field.

Walls

The Norris-Reynolds one-equation model was used near the walls and on the walls all quantities were set to zero except for the pressure, temperature and dissipation rate for which the gradients normal to it were set to zero.

THE CALC-BFC CODE

Basics

In this report a finite volume computer program – CALC-BFC (Boundary

- Fitted - Coordinates) — for three-dimensional complex geometries has been used. A detailed description of the code is given in [4] and some of its main features are briefly discussed below.

The **SIMPLEC** solution algorithm [14] is used and the program uses Cartesian velocity components, collocated variables situated in the middle of the control volume and linear interpolation when a variable is needed at a face of the control volume. The convective terms are discretized using both a hybrid upwind/central differencing scheme, as well as a second order accurate bounded scheme of van Leer [11]. The diffusive terms are discretized using central differences, which are of second order accuracy. For the time derivatives a second order accurate scheme, referred to as the Crank-Nicolson scheme has been used. All these schemes, except for that of van Leer which will be shortly discussed below, are described in [14].

When using collocated variables instead of a staggered grid-arrangement for the velocities, special care must be taken when the velocities are interpolated from the nodes to the control volume faces in order to avoid non-physical oscillations. This is due to the weak coupling between the velocity component at the face and the corresponding pressure gradient. Rhie and Chow [16] solved this problem.

The van Leer Scheme [11]

For steady-state flows the van Leer scheme proceeds as follows. First identify the upstream (**U**), downstream (**D**) and centrally located (C) nodes for each cell face on the basis of the sign of the cell face velocity. Thus, referring to **Figure 2** below, if $U_{i+1/2,j}$ is positive, set $\Phi_U = \Phi_{i-1,j}$, $\Phi_D = \Phi_{i+1,j}$ and $\Phi_C = \Phi_{i,j}$. Then if

$$|\Phi_D - 2\Phi_C + \Phi_U| \geq |\Phi_D - \Phi_U| \tag{27}$$

set

$$\Phi_{i+1/2,j} = \Phi_C \tag{28}$$

otherwise set

$$\Phi_{i+1/2,j} = \Phi_C + \frac{(\Phi_D - \Phi_C)(\Phi_C - \Phi_U)}{(\Phi_D - \Phi_U)} \tag{29}$$

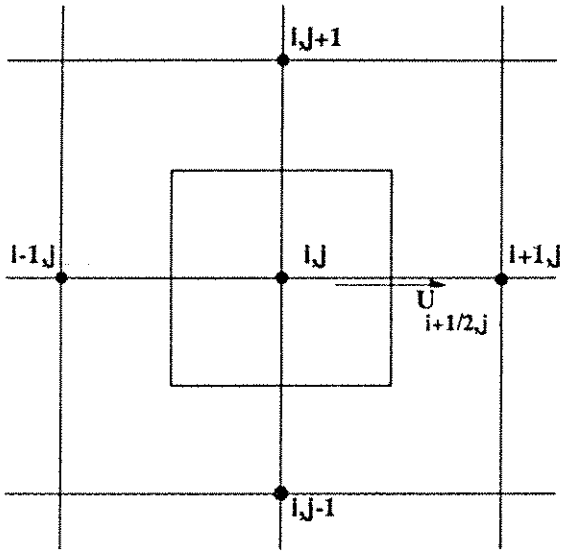

Figure 2. Grid geometry.

This scheme is a first-order upwind scheme with a correction term which gives second-order accuracy. All the momentum equations may be solved by the van Leer scheme, and also the turbulent equations. This bounded scheme prevents occurence of negative values of k and ε. Such values are not only unrealistic, but destabilize the turbulence equations and prevent the solution from converging.

RESULTS AND DISCUSSION

The calculations of the two-dimensional turbulent flow have been carried out for two different lip-to-slot ratios (t/s=**0.1** and **1.0**) and for two different velocity ratios (M=**1.0** and **1.5**). The bulk temperature in the slot, T_s was approximately $40°C$ and in the freestream the temperature, T_g was **23**-$-29\ °C$. Since the temperature differences are quite small, and hence the bouyancy effects should be negligible compared with the convection terms, it was assumed that the temperature had no influence on the velocity field.

The outlet boundary condition was set **50**$-$**80** slot-heights downstream of the lip in order to be sure that the vortex shedding has dissipated, and hence the streamwise gradients could be set to zero. The upper boundary was set **5**$-$**12** slot-heights over the wall, in order to be able to accept a symmetry condition. More details on the results can be found in Jansson [6].

Case t/s=0.1. Steady Calculations.

The calculations in this case were performed at two different Reynolds numbers (**12550** and **18950**) based on the slot-height, s and the mean velocity in the slot, U_s. The lip itself causes little disturbance, and the flows will interact as two merging shear-layers and not as a turbulent wake. For this case, the downstream effects of the lip are primarly due to the difference in velocity between the two flows. Steady solutions were obtained no matter

which of the turbulence models were used. The total grid consisted of **190×80** grid points.

Since the experimental study used hot-wire equipment, the measured velocity has contributions from the components in both the x- and y-direction. The calculated velocities in **Figures A1** and **A2** are therefore the absolute ones. The agreement is good between calculations and measurements considering mean velocities for both turbulence models.

The dimensionless mean temperatures are shown in **Figures A3** and **A4** and the agreement between calculations and measurements is good in both the free stream and the mixing layer. The mean flow does not seem to penetrate much into the slot flow, which results in a high film cooling effectiveness near the wall. This low mixing of the flows is probably due to the fact that the thin lip creates very little vortex shedding and hence the periodic fluctuation, which is important for the mixing process, is small. The diffusion term in the temperature equation was calculated using Boussinesq approximation:

$$\frac{\partial}{\partial x_i}\left[\left(\frac{\mu}{\sigma}+\frac{\mu_t}{\sigma_t}\right)\frac{\partial T}{\partial x_i}\right] \tag{30}$$

where σ and σ_t are the laminar and the turbulent Prandtl numbers. The value of the turbulent Prandtl number was set to **0.9** in the near-wall region and **0.5** elsewhere. The latter value has been found to be appropriate for plane jets, wakes and mixing layers [20]. At the wall (y/s=0), the results come together in a single point at θ around unity in the region near the lip, but θ decreases for higher x/s. The calculated profiles in the last position indicate that the lateral mixing is too large in the calculations. The grid expands in the streamwise direction and at this position it is quite coarse, which in turn leads to numerical diffusion, and the profiles being smeared out. Except for the last position considered, the film cooling effectiveness at the wall is generally well predicted.

Case t/s=1.0. Unsteady Calculations.

The calculations at this case (Re_s =12400), resulted in unsteady motions. This unsteady behaviour of the flow is due to vortex stretching, with vorticies alternatively shedding from the upper and lower edges of the lip, forming a periodic von Kárman vortex sheet behind it. To illustrate the periodicity of the flow the pressure contours at different times during a whole cycle are shown in **Figure B1**. At the lower edge of the lip, a vortex has just been created and is convected downstream as time increases. During its transport it will continuously lose vorticity, which can be seen by the increasing distance between the isobars in the vortex. All the unsteady calculations presented here were calculated using the Crank-Nicolson time discretization scheme, and both the hybrid upwind/central differencing scheme and

the scheme of van Leer was used for the convective terms. The grid consisted of **190×144** grid points. The total time of a cycle was almost 2.5 ms and has been divided into approximately 90 timesteps of Δt=25 μs in the calculations, which gave a Strouhal number, Sr:

$$Sr = \frac{f \cdot t}{\overline{U}_s} \approx 0.22 \tag{31}$$

At high Reynolds numbers three-dimensional stochastic turbulent fluctuations are superimposed on the periodic unsteady motion. The instantaneous velocity component, U_i is separated into time-mean velocity components, $\overline{U}_i$, periodic fluctuating components, $\widetilde{U}_i$ (together called phase averaged, $\langle U_i \rangle$) and turbulent fluctuating components, u_i, i.e.:

$$U_i = \overline{U_i} + \widetilde{U}_i + u_i = \langle U_i \rangle + u_i \tag{32}$$

where $\langle U_i \rangle$ is the velocity resolved by the numerical method. The time-averaged mean velocities in the calculations are shown in **Figures B2** and **B3**. With the use of the $k - \varepsilon$ model, the results obtained using the van Leer scheme are in considerably better agreement with the measurements than those obtained by using the hybrid scheme. The **ASM** predicts the flow field better than the $k - \varepsilon$ model, but when the van Leer scheme is used, both models are capable of predicting the flow quite well.

From **Figure B4**, it can be seen that the $k - \varepsilon$ model leads to greater turbulent fluctuations than the **ASM** in the wake region. This overprediction of turbulent kinetic energy results in excessive eddy viscosity, which damps the periodic fluctuations, and hence the mixing process. The measured values are the sum of the periodic and the turbulent fluctuations. The corresponding calculated fluctuations time-averaged over a whole cycle $\overline{u_{TOT}}$ are computed as:

$$\overline{u_{TOT}} = \frac{1}{n} \sum_{m=1}^{n} \left[\left| \langle U \rangle_{abs} - \overline{U}_{abs} \right| + u_{abs} \right]_m \tag{33}$$

where n is the number of timesteps during one cycle. It can be seen from **Figure B4** that the contribution from the periodic fluctuations is quite high near the lip, but further downstream this periodic contribution decreases, indicating that the strength of the vortex sheet decreases. The fluctuations in the free stream are in better agreement with the measurements when the van Leer scheme is used. The reason is that the van Leer scheme is less diffusive (second-order accurate) compared with the hybrid scheme (first-order accurate) and this results in a stronger vortex shedding, which gives a better vertical mixing between the two flows.

In **Figure B5** the time-averaged dimensionless mean temperature profiles are shown, and it can again be noted that the van Leer scheme results in a better mixing. Considering the same discretization scheme and comparing the turbulence models, it can be seen that in the **ASM** case, the profiles are a little bit more smeared and better predicted than those obtained in the $k - \varepsilon$ case. This is a result of the higher momentum exchange from the mean flow in the y-direction and hence the main and slot flows are more mixed when the **ASM** is used. In the near wall region, the calculated film-cooling effectiveness is generally too high, which means that the flow in the free stream does not penetrate far enough into the slot flow, indicating that the calculated vortex shedding is too weak. Further downstream, the film cooling effectiveness is decreased, owing to the increased mixing of the flows, which acts to destroy the "heating" film. It should be noted that in the calculations as well as in the measurements, the wall was assumed to be adiabatic, and that the "hot" flow was in the slot.

There were some difficulties in comparing the calculations with the measurements, since the temperature in the free stream varied from day to day during the measurements. This means that the temperature in the free stream during the measurement of a temperature profile at a downstream location varied from the free stream temperature during the measurements at another location. In the calculations using the **ASM**, the diffusion term was approximated by the following gradient-type expression [9]:

$$-\overline{u_i\theta} = C_\theta \frac{k}{\varepsilon} \overline{u_i u_j} \frac{\partial T}{\partial x_j} \tag{34}$$

where the constant C_θ was taken as **0.11**.

CONCLUDING REMARKS

Finally, the following conclusions can be drawn:

- Both turbulence models predict the mean flow field quite correctly when the lip is thin (**t/s=0.1**) and no streamline curvature effects are present.
- When the lip is thick (**t/s=1.0**) and hence the flow becomes unsteady, it is of great importance that a fine grid in space (or a higher order scheme) is used to achieve good agreement with experiments.
- In the unsteady cases, where streamline curvature effects are present, the anisotropic behaviour of the turbulence is better predicted by the **ASM** than by the $k - \varepsilon$ model. The calculated film cooling effectiveness at the wall is too large, indicating that the penetration of the cold flow in the free stream into the slot is too weak.

Appendix A. Case t/s=0.1. Steady calculations.

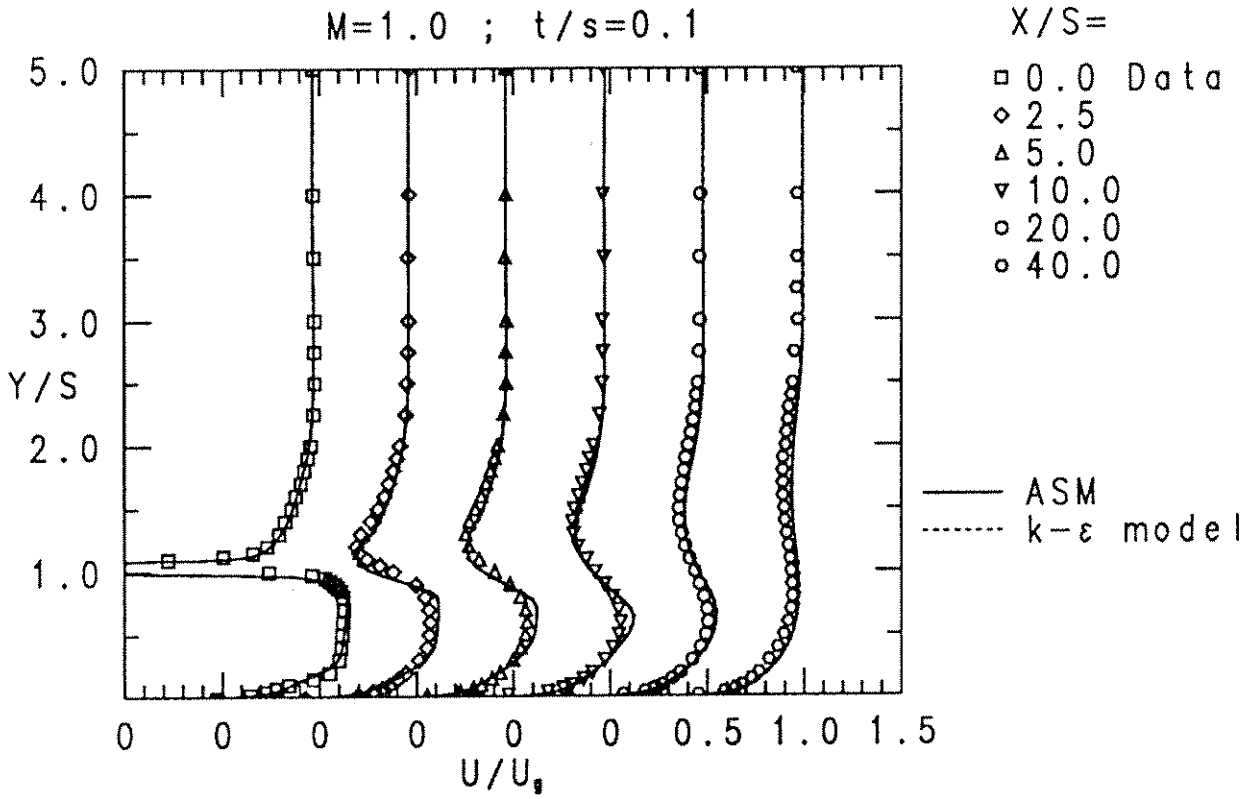

Figure A1. Mean velocity profiles, M=1.0, t/s=0.1.

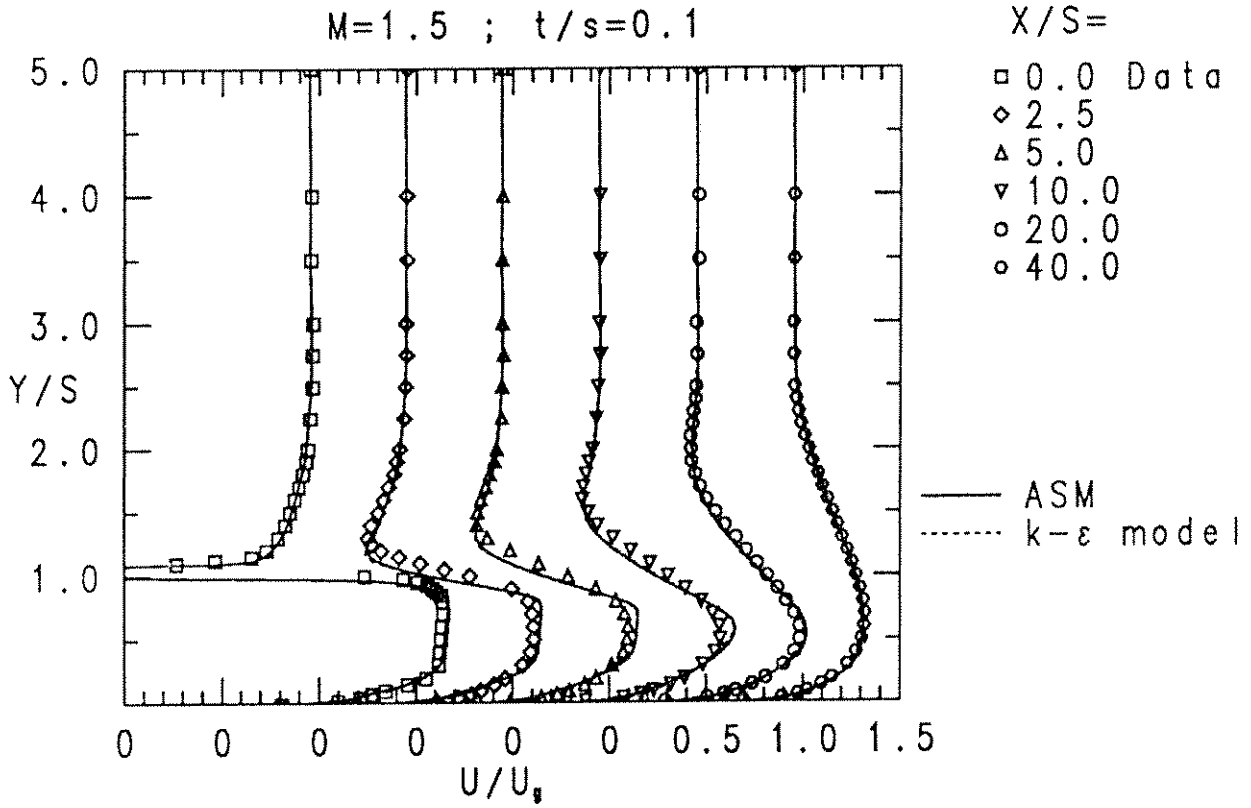

Figure A2. Mean velocity profiles, M=1.5, t/s=0.1.

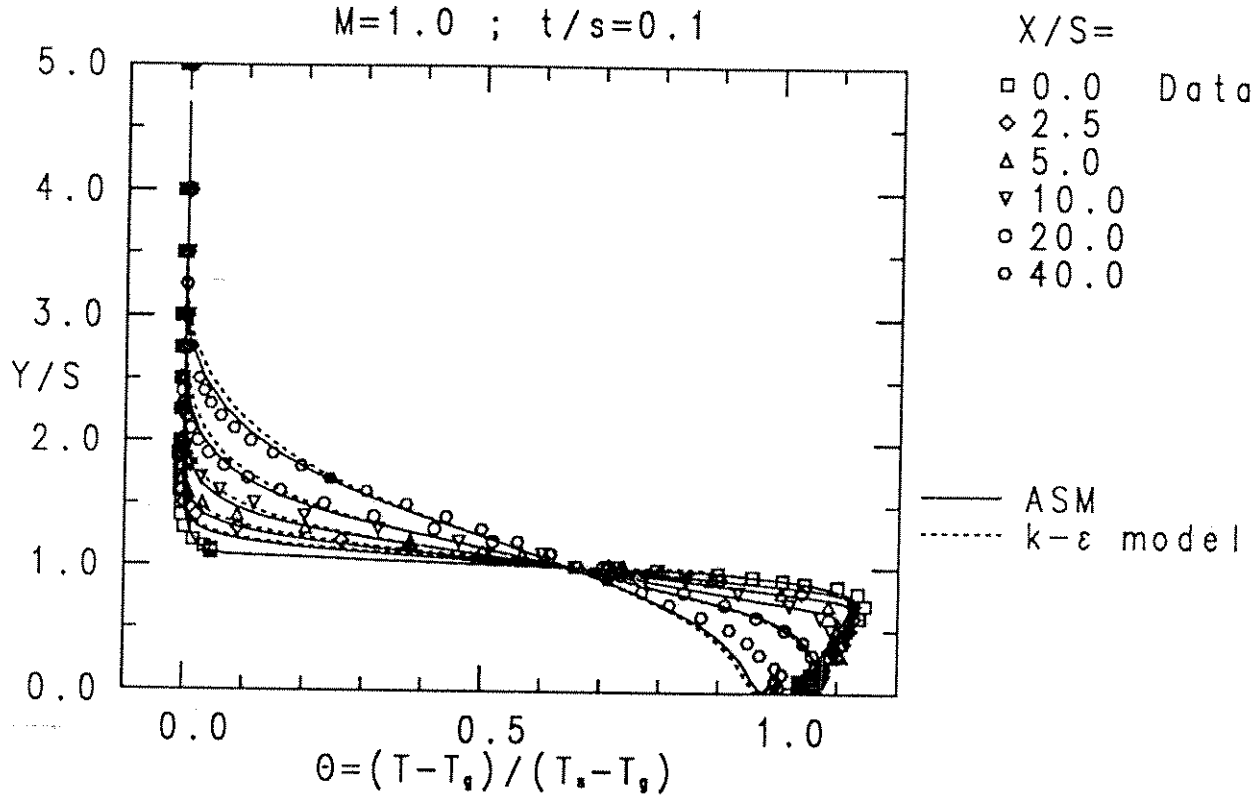

Figure A3. Film-cooling effectiveness, M=1.0, t/s=0.1.

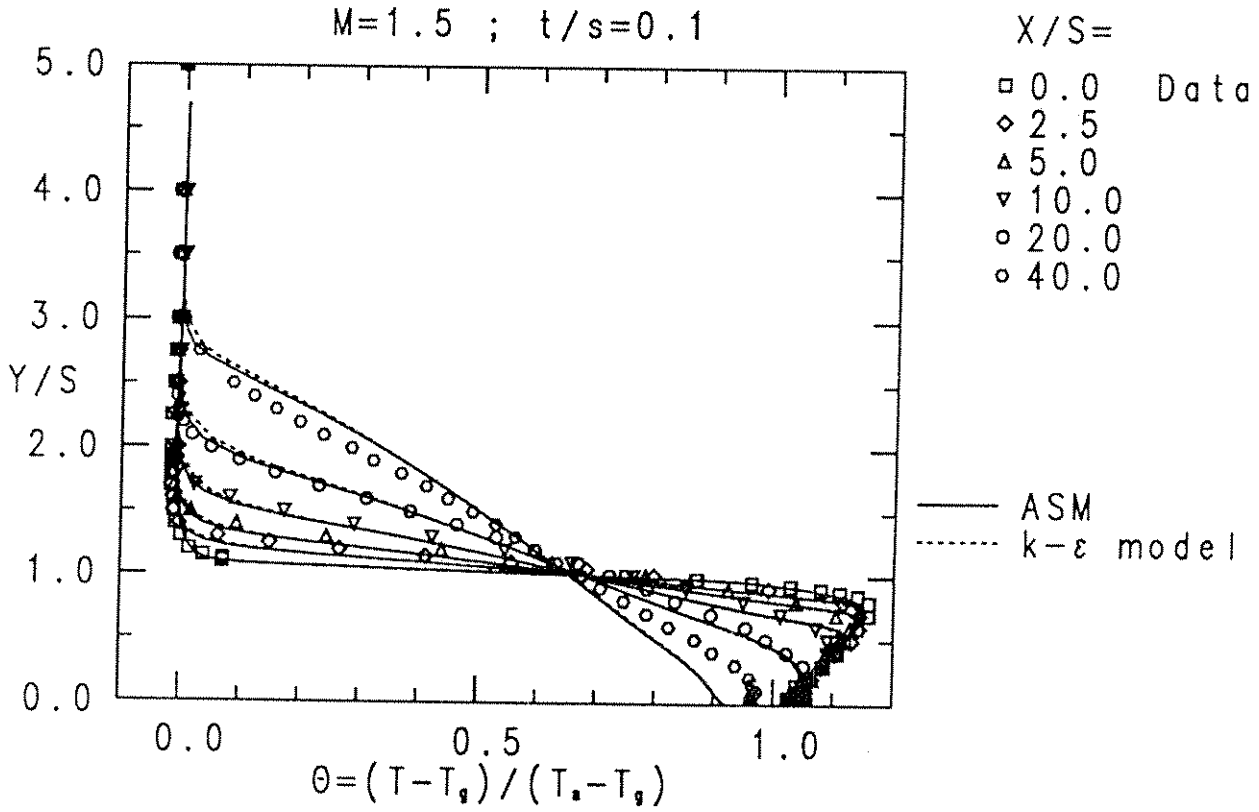

Figure A4. Film-cooling effectiveness, M=1.5, t/s=0.1.

Appendix B. Case t/s=1.0. Unsteady calculations.

t/T=0

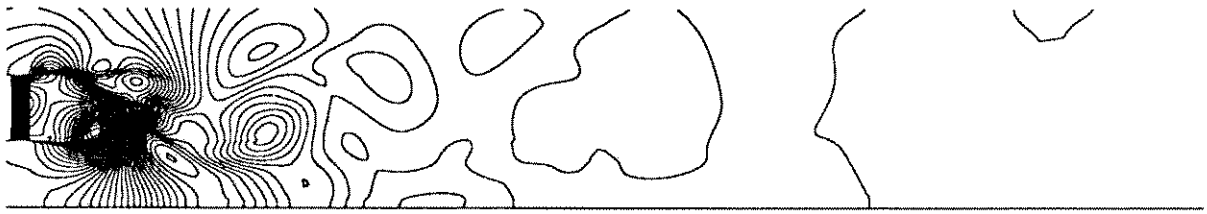

t/T=10/47

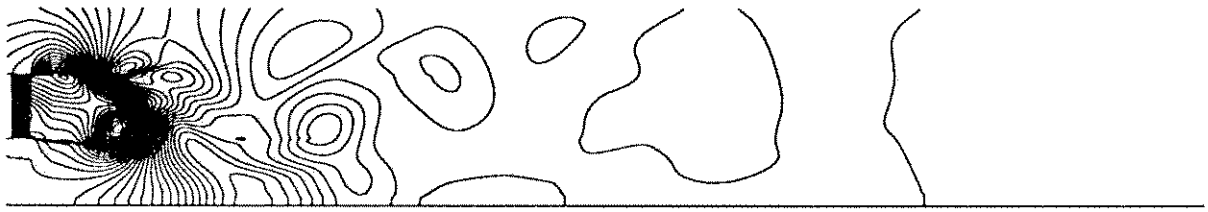

t/T=20/47

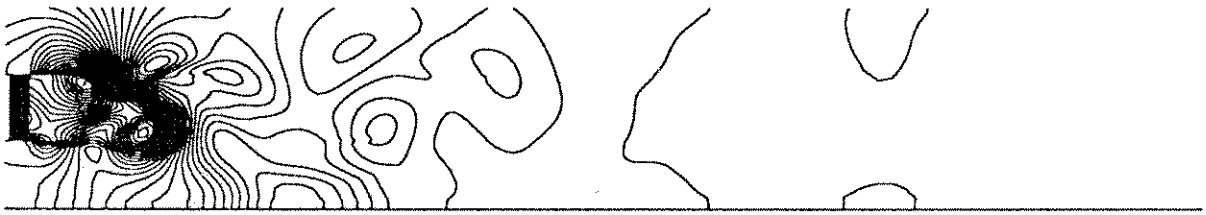

t/T=30/47

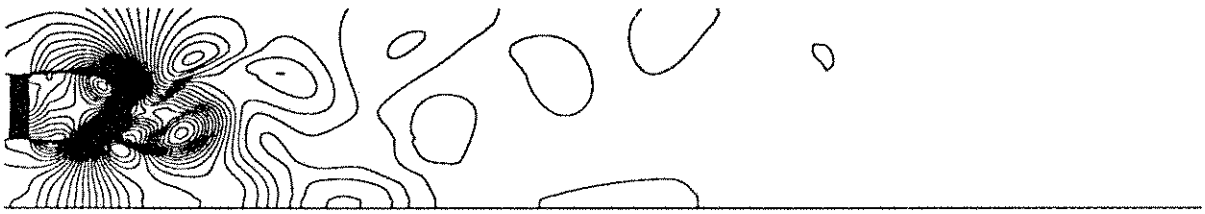

t/T=40/47

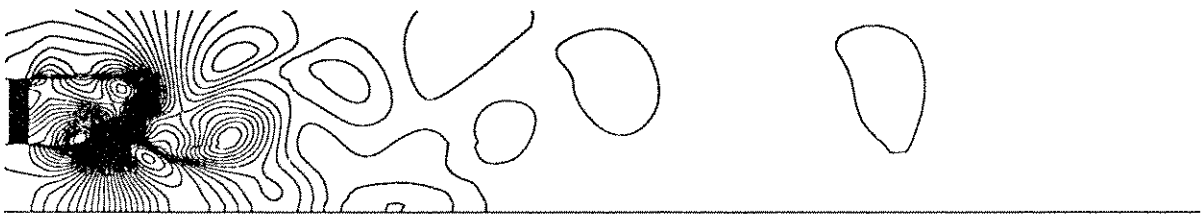

t/T=50/47

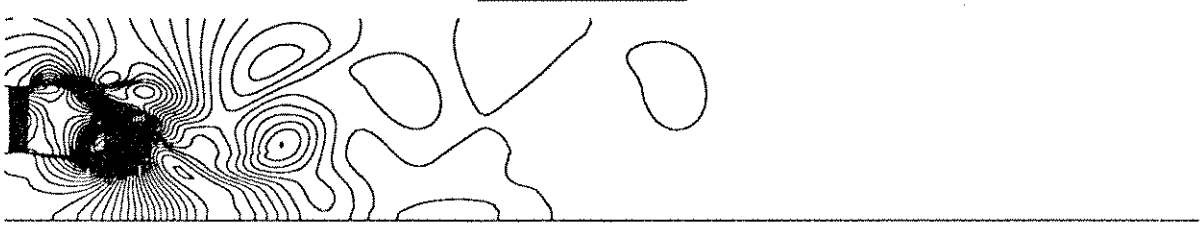

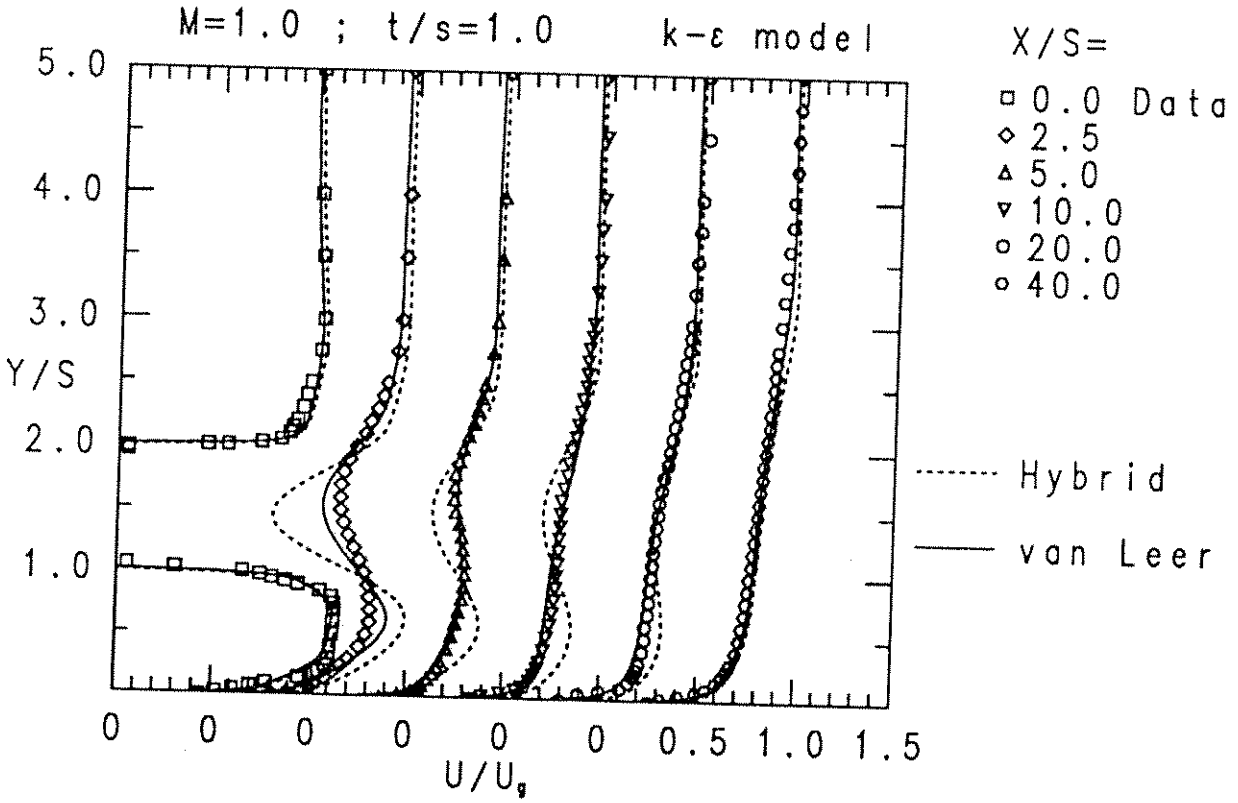

Figure B2. Time-averaged mean velocity profiles, $k-\varepsilon$ model.

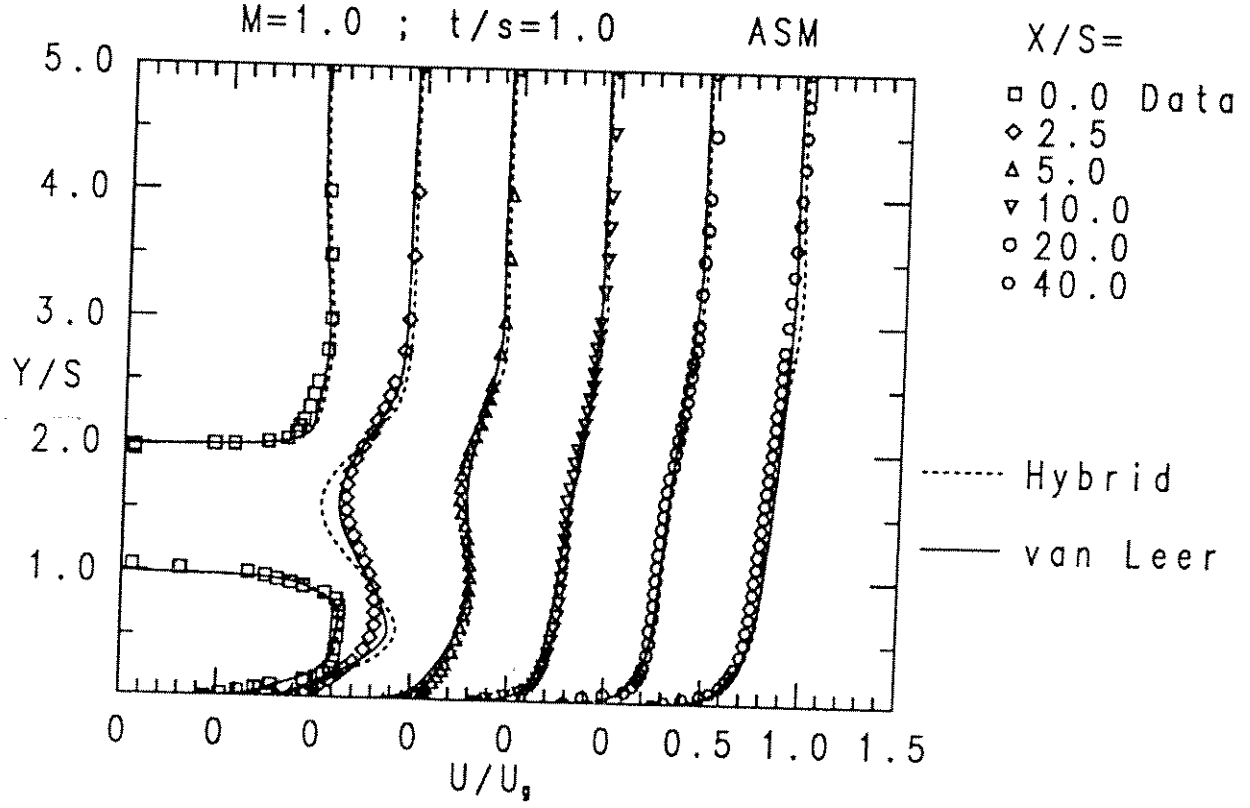

Figure B3. Time-averaged mean velocity profiles, ASM.

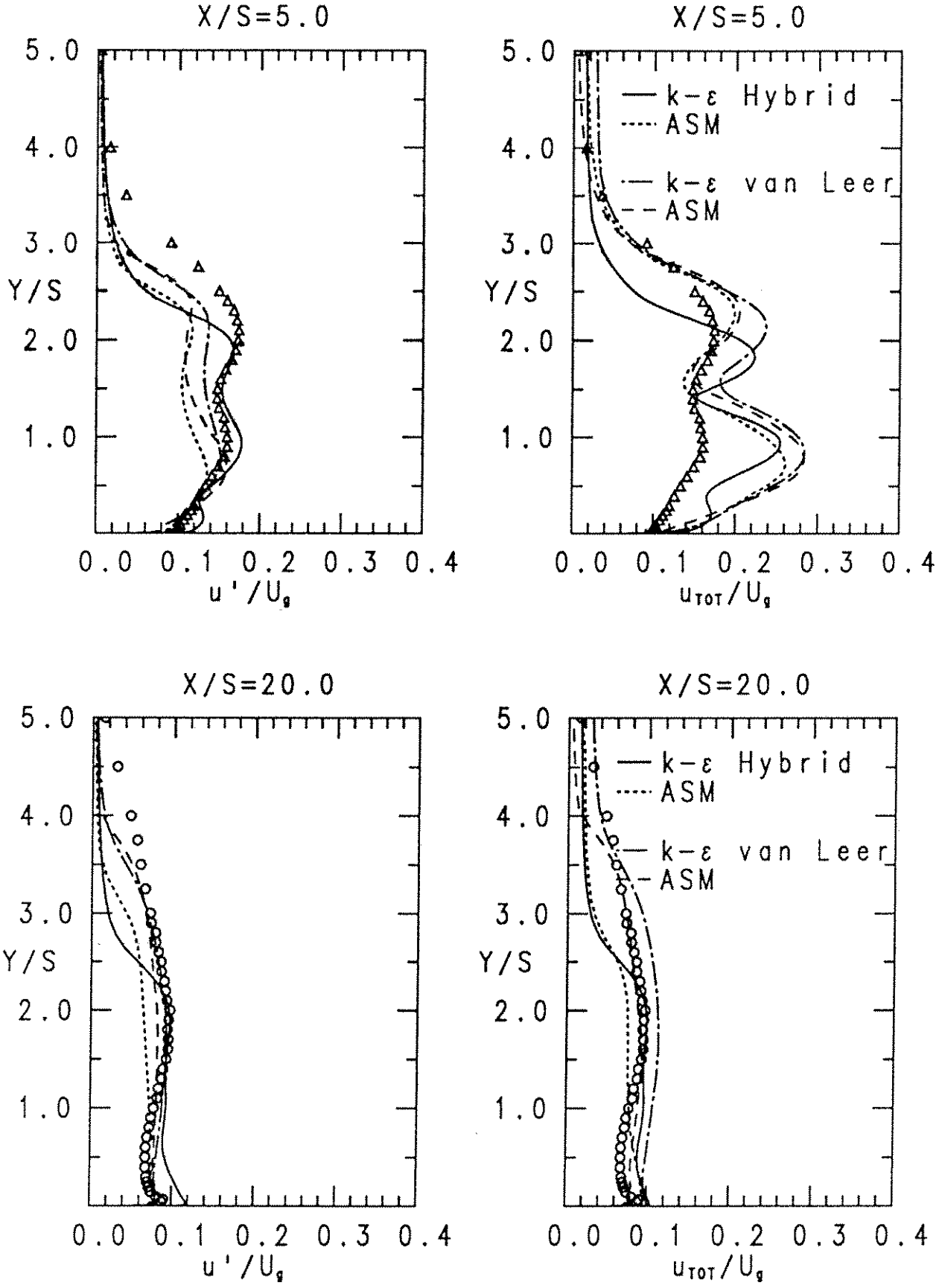

Figure B4. Turbulent $(\overline{u}/U_g)$ and total $(\overline{(u+\widetilde{U})}/U_g)$ velocity fluctuations. Markers denote measurements.

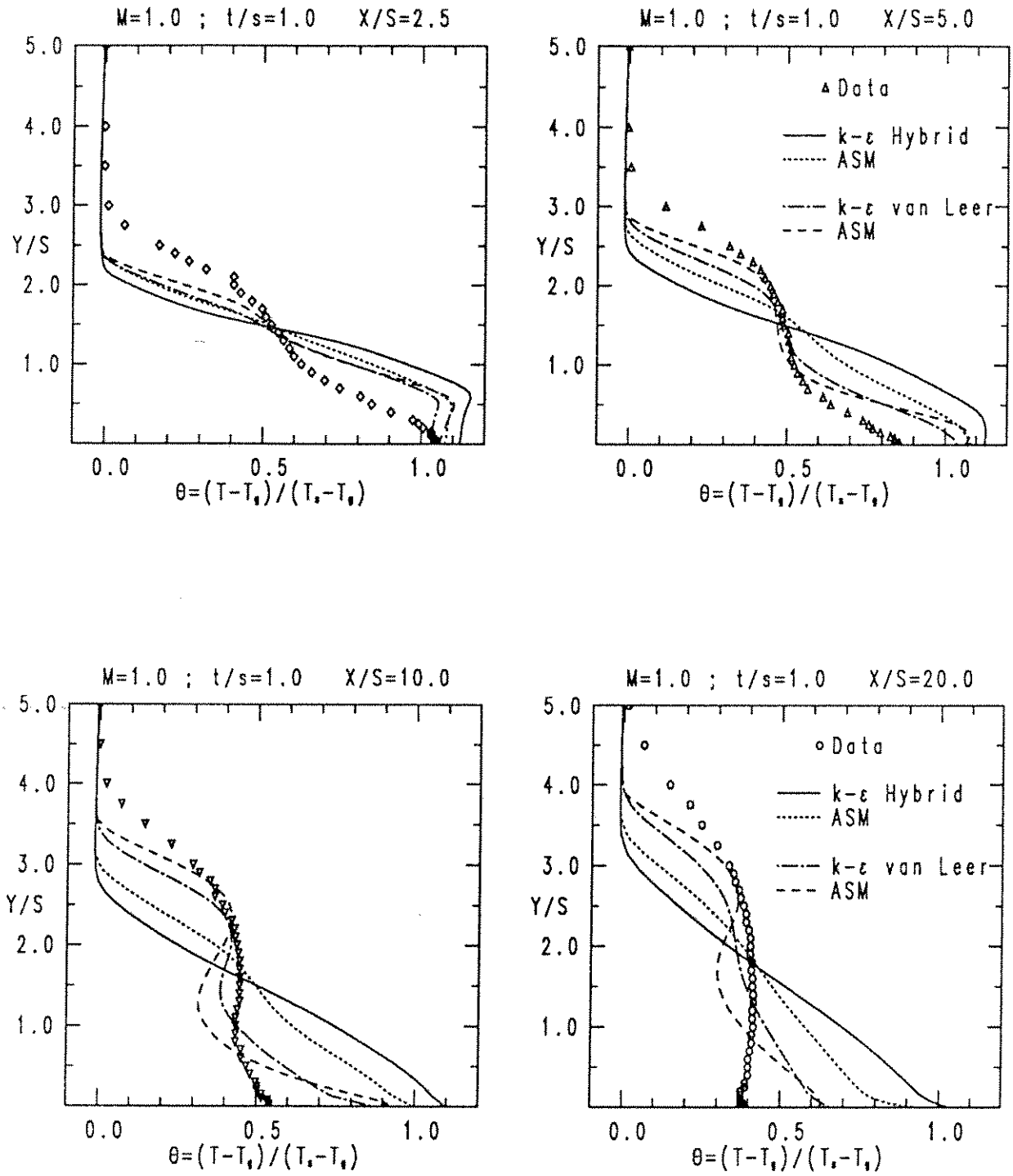

Figure B5. Film-cooling effctiveness at different positions.

REFERENCES

1. **Boman, U. and Olsson, E.**, "The influence of high lip-to-slot-thickness on film cooling effectiveness", Licentiate of Engineering Thesis, Department of Thermo and Fluid Dynamics, Chalmers Univ. of Tech., Gothenburg, 1990.

2. **Chen, H.C. and Patel, V.C.**, "Near-wall turbulence models for complex flows including separation", *AIAA J.*, **26**, pp. 641-648, 1988.

3. **Cordes, J.**, "Entwicklung und Anwendung eines Zweischichten-Turbulenzmodells für abgelöste zweidimensionale Strömungen", Ph.D. Thesis, University of Karlsruhe, 1991.

4. **Davidson, L.**, CALC-BFC: "A finite-volume code for complex three-dimensional geometries using collocated variables and cartesian velocity components", Rept., Dept. of Applied Thermodynamics and Fluid Mechanics, Chalmers Univ. of Techn., Gothenburg, 1989.

5. **Huang, P.G. and Leschziner, M.A.**, "Stabilization of recirculating flow computations performed with second-moment closures and third-order discretization", Proceedings of the 5th Symp. on Turb. Shear Flows, Cornell,1985.

6. **Jansson, S., Davidson, L. and Olsson, E.**, "Numerical investigation of steady and unsteady flows comparing turbulence models and different near-wall models", Licentiate of Engineering Thesis, Department of Thermo and Fluid Dynamics, Chalmers Univ. of Tech., Gothenburg, 1992.

7. **Kacker, S.C. and Whitelaw, J.H.**, "Predictions of wall-jet and wall-wake flow", *J. Mech. Eng. Sc.*, **12**, no. 6, pp. 404-419, 1970.

8. **Launder, B.E.**, "Low-Reynolds number turbulence near walls", Rept. TFD/86/4, UMIST, Dept. of Mech. Eng., Manchester, 1986.

9. **Launder, B.E.**, "Turbulence models and their experimental verification: 11. Scalar property transport by turbulence", Imperial College Mech. Eng. Dept., Rept. HTS/73/26, 1973.

10. **Launder, B.E. and Rodi, W.**, " The turbulent wall jet - — measurements and modelling", *Ann. Rev. Fluid Mech.*, **15**, pp. 429-459, 1983.

11. van Leer, B., "Towards the ultimate conservative difference scheme. monotonicity and conservation combined in a second order scheme", *J. Computational Physics*, Vol. **14**, pp. 361, 1974.

12. Naot, D., Shavit ,A. and Wolfshtein, M., "Interactions between components of the turbulent velocity correlation tensor due to pressure fluctuations", *J. of Technology*, **Vol. 8**, pp. 259, 1970.

13. Norris, L.H. and Reynolds, W.C., "Turbulent channel flow with a moving wavy boundary", Rept. No. FM-10, Dept. Mech. Eng., Stanford University, 1975.

14. Patankar, S.V., "Numerical heat transfer and fluid flow", McGraw-Hill, Washington, 1980.

15. Patel, V.C., Rodi, W. and Scheurer, G., "Turbulence models for near-wall and low-Reynolds number flows: A review", *AIAA J.*, **23**, pp. 1308-1319, 1985.

16. Rhie, C.M. and Chow, W.L., "Numerical study of the turbulent flow past an airfoil with trailing edge separation", *AIAA J.*, **21**, pp. 1527-1532, 1984.

17. Rodi, W., "Experience with Two-Layer Models Combining the $k - \varepsilon$-model with a One-Equation Model Near the Wall", *AIAA J.*, 29th Aerospace Sciences Meeting, January 7-10, Reno, Nevada, 1991.

18. Rodi, W. and Scheurer, G., "Calculation of Curved Shear Layers with Two-Equation Turbulence Models", *Phys. Fluids*, **26**, No. 6, pp. 1422-1435, 1983.

19. Rotta, J.C., "Turbulente Strömungen", B.G Teubner, Stuttgart, 1972.

20. Spalding, D.B. and Patankar, S.V., "Heat and mass transfer in boundary layers", pp. 21, Morgan-Grampian Books, London, 1967.